Continuum Modelling of Shear-Coupled Grain Boundary Migration

Stéphane Berbenni, Bhasker Paliwal and Mohammed Cherkaoui

Abstract The deformation accommodation mechanisms associated to grain boundaries (GBs) significantly affect the mechanical behavior of nano-polycrystals. Among these mechanisms, stress-induced GB migration is now seen to compete or interplay with other intra-granular and GB mechanisms in a wide range of temperatures. A complete micromechanics-based model is here proposed using the concepts of continuum thermodynamics and kinematics to derive a new constitutive model able to describe stress-induced GB migration. Like non diffusive phase-transformations, stress-induced GB migration can be considered on the thermodynamics point of view of conservative nature (diffusionless but thermally activated) until high temperature with respect to melting point. Here, in the framework of continuum micro-mechanics which should be easily implemented in a polycrystalline model, we will first describe the micromechanical framework: the kinematics and the thermodynamics associated with additive mechanisms including plastic deformation in the bulk crystals, GB migration and GB sliding. For the sake of illustration of the present general theory, we will focus on planar bi-crystals and only perfect shear-coupling GB migration situations of [001] symmetric tilt GBs in Cu. Numerical examples and responses of

S. Berbenni (✉)
Laboratoire d'Etudes des Microstructures et de Mécanique des Matériaux, LEM3,
UMR CNRS 7239, University of Lorraine, 57045Metz, France
e-mail: stephane.berbenni@univ-lorraine.fr

S. Berbenni · B. Paliwal · M. Cherkaoui
Unité Mixte Internationale Georgia Tech Lorraine-CNRS, UMI CNRS 2958,
57070 Metz, France B. Paliwal
e-mail: bpaliwal@gatech.edu

M. Cherkaoui
e-mail: mcherkaoui@me.gatech.edu

B. Paliwal · M. Cherkaoui
George W. Woodruff School of Mechanical Engineering, Georgia Institute of Technology,
30332-0405Atlanta 22, GA, USA

H. Altenbach et al. (eds.), *Generalized Continua as Models for Materials*,
Advanced Structured Materials 22, DOI: 10.1007/978-3-642-36394-8_3,

the micromechanical model are given for these bi-crystals considering both isotropic and anisotropic elasticity. These ones are fed by computer-aided MD simulations for which deformation mechanisms are identified.

1 Introduction

"Shear-coupled" grain boundary (GB) migration is now seen to compete or interplay with other intra-granular GB mechanisms in a wide range of temperatures [1, 2]. In nanocrystalline (NC) metals, it now becomes challenging to understand stress-induced GB migration because this is thought to enhance grain growth at low temperatures, which is important for making stable structural materials for engineering applications. In these materials, the interplay of GB migration with other possible GB deformation mechanisms like GB sliding [3] becomes very complex due to the high GB volume fraction. The mechanism of stress-induced shear-coupled GB migration at room temperature is today well identified by a shear deformation accompanying GB migration for symmetric (coincident) tilt GB (here denoted STGB) but less for general non symmetric GB. This new deformation mechanism is different from strain-induced GB migration studied for recrystallization phenomena. The latter essentially comes from spatially heterogeneous intra-crystalline dislocation densities in the vicinity of GB.

Theoretical studies [4] as well as molecular dynamics (MD) simulations using the EAM potential for Cu bicrystals with STGB [1, 2, 5] show that stress-induced GB migration is characterized by a shear "coupling factor" (or shear deformation usually denoted β) which is defined by the ratio of the shear displacement parallel to the GB plane to the GB propagation normal to its plane. This coupling factor is purely geometric and depends on the tilt GB misorientation. "Shear-coupled" GB migration was recently analyzed by [1, 2] using the "Frank-Bilby" equation [6–8]. Due to the high resolved shear stresses required to move STGB [1, 2, 5, 9], it is expected that GB migration would play a key role in the understanding of inverse Hall-Petch effect in addition to GB sliding or GB dislocation nucleation-propagation-absorption.

Due to the complexity of atomistic mechanisms in the case of general GB, we will limit the present study to the constitutive behavior of Cu STGB undergoing shear-coupled migration. For Cu [001] STGB, two shear deformation modes associated to $<110>$ and $<100>$ crystallographic directions linked to two coupling factors (resp. negative and positive) were observed using MD simulations and confirmed experimentally by [10]. In particular, a dual temperature dependent behavior for certain misorientations (around 53°) may be observed at finite temperatures. According to [1], a transition exists above 800 K, where the shear-coupled GB migration may be interrupted by occasional sliding events. Between these sliding events, the GB plane continues to move accompanied by shear. This suggests that pure GB sliding occurs through atomistic mechanisms that preserve GB character. At medium and low temperatures, shear-coupled GB migration has a stick slip stress versus time characteristic response which can be retrieved by atomistic simulations [11, 12].

The objective of the present contribution is to provide a complete micromechanics-based constitutive model using the concepts of continuum mechanics to describe shear-coupled GB migration in bi-crystals. Kinematics and thermodynamics associated with different additive dissipative mechanisms will be introduced in Sect. 2. Here, shear-coupled GB migration will be considered as a shear process in the local coordinates associated to grain boundary plane that can be described in linearized kinematics by an *eigenstrain* (or plastic strain jump at the discontinuity GB surface) similarly to deformation twinning [13]. To illustrate the present theory, Sect. 3 will focus on bi-crystals with plane GB and pure shear-coupled GB migration situations without sliding in addition to intra-crystalline plastic deformation. It will be derived that the shear "coupling factor" β is related to plastic strain jump at the GB surface through an "orientation tensor" characterized by GB surface dislocation Burgers vector and slip plane. In Sect. 4, numerical examples and MD simulations will be restricted to the shear responses of three Cu STGB exhibiting shear-coupled GB migration with absence of bulk intra-crystalline plasticity (because crystal sizes are lower or equal to $10\,\mathrm{nm}$). In these situations, atomic scale deformation mechanisms are well identified using the concept of "displacement shift complete" (DSC) dislocations [14, 1] or "disconnections" [15]. These interfacial defects will be introduced in the constitutive framework and a discussion about the role of stress-induced GB migration coupled with anisotropic elasticity on stress-strain characteristics is provided in the light of the micromechanics-based model. Section 5 concludes and sketch some perspectives for the applicability of the present bi-crystal constitutive framework in mean field polycrystalline modeling involving NC materials and/or deformation twinning.

Throughout the paper, a "," indicates a spatial differentiation, a superposed dot a particle time derivative (or rate). "[A]" denotes the jump of a bulk field "A" at a discontinuity surface such that $[\mathrm{A}] = \mathrm{A}^{\mathrm{II}} - \mathrm{A}^{\mathrm{I}}$ to be consistent with Fig. 1, where I and II are both crystals forming a bicrystal (crystal II being the consumed crystal during interface motion). "$\langle \mathrm{A} \rangle$" denotes the average of a bulk field A across the interface defined by $\langle \mathrm{A} \rangle = \frac{1}{2}\left(\mathrm{A}^{\mathrm{II}} + \mathrm{A}^{\mathrm{I}}\right)$. The Einstein summation convention is also used throughout the paper.

2 Continuum Modeling

2.1 Kinematics

Following [16–18], the particle velocity vector jump at the internal discontinuity surface (GB) denoted hereafter S can be decomposed as follows (Fig. 1)

$$[v_i] = [v_i]^{(1)} + [v_i]^{(2)}, \tag{1}$$

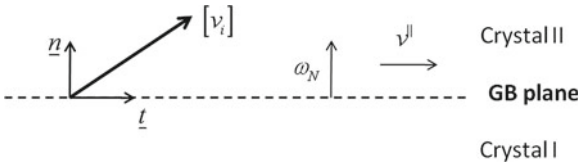

Fig. 1 Schematic representation of grain boundary (GB) migration and sliding (kinematics). $[v_i] = v_i^{II} - v_i^{I}$ denotes the jump of v_i at the interface (GB plane) oriented by unit normal vector n_i from crystal I to crystal II

where

$$[v_i]^{(1)} = -[u_{i,j}]\, n_j \omega_N \tag{2}$$

is the particle velocity jump due to normal GB propagation assuming linearized kinematics [19, 16] and $[v_i]^{(2)}$ is the part of particle velocity jump at the discontinuity surface due to tangential GB sliding.

In Eq. (2), $[u_{i,j}]$ represents the jump of displacement gradient or total distortion at the discontinuity surface S. ω_N is the GB normal velocity and n_i is the unit normal vector to the GB plane oriented from I towards II (Fig. 1). According to Fig. 1, the particle velocity jump contains a tangential part $v^{\parallel}$ and a normal one $v^{\perp}$ as follows

$$[v_i] = v^{\parallel} t_i + v^{\perp} n_i, \tag{3}$$

where $v^{\parallel}$ reads

$$v^{\parallel} = \beta \omega_N + v_s \tag{4}$$

In Eq. (4), $v_s = [v_i]^{(2)}\, t_i$ is the tangential velocity due to GB sliding. Furthermore, β is a purely geometric parameter that can be identified as the "coupling factor" following the terminology used by [4]. Using Eq. (2), β can be identified as a function of the interfacial jump of displacement gradient through the following expression

$$\beta = -[u_{i,j}]\, n_j t_i \tag{5}$$

It is noteworthy that Eq. (5) was postulated by [4] without any direct link to continuum-based kinematics like in the present contribution.

2.2 Thermodynamics

The mechanical dissipation D in the body V is defined as the difference between the power of the applied forces denoted P_{ext} and the rate of change of the stored energy $\dot{\Phi}$ (time derivative of the Helmholtz free energy), which corresponds under isothermal and quasi-static evolutions to the time derivative of the elastic energy [20, 21]

$$D = P_{ext} - \dot{\Phi} \tag{6}$$

Neglecting the excess interfacial energy effects at GB in Eq. (6), Φ is given by

$$\Phi = \int_V \frac{1}{2}\sigma_{ij}\varepsilon^e_{ij}\,dV, \tag{7}$$

where σ_{ij} and ε^e_{ij} are respectively the Cauchy stresses and the elastic strains.

The power of external forces is defined as

$$P_{ext} = \int_{\partial V} \sigma_{ij} n_j v_i\,dV, \tag{8}$$

where n_j is the unit outward normal vector at a point of the external boundary of V denoted ∂V and v_i is the material velocity at this point.

As described in the kinematics part (Sect. 2.1), the strains and stresses are discontinuous across the moving interface. Consequently, the elastic energy density $\varphi = \frac{1}{2}\sigma_{ij}\varepsilon^e_{ij}$ present in Eq. (7) is also discontinuous through the moving discontinuity surface S. Applying the transport theorem for growing discontinuity surface S to Eq. (7), $\dot{\Phi}$ is given by

$$\dot{\Phi} = \int_V \dot{\varphi}\,dV - \int_S [\varphi]\omega_N\,dS. \tag{9}$$

In Eq. (9), the first volume term containing $\dot{\varphi}$ can be easily computed using $\varepsilon_{ij} = \varepsilon^e_{ij} + \varepsilon^p_{ij}$ as follows

$$\int_V \dot{\varphi}\,dV = \int_V \sigma_{ij}\left(\dot{\varepsilon}_{ij} - \dot{\varepsilon}^p_{ij}\right)dV. \tag{10}$$

The second term of Eq. (9) which contains $[\varphi]$ is defined as

$$[\varphi] = \frac{1}{2}\left(\sigma^{II}_{ij}\left(\varepsilon^{II}_{ij} - \varepsilon^{pII}_{ij}\right) - \sigma^{I}_{ij}\left(\varepsilon^{I}_{ij} - \varepsilon^{pI}_{ij}\right)\right). \tag{11}$$

This expression is much simplified in the case of linear homogeneous elastic properties and using the usual symmetries of the homogeneous elastic stiffness tensor C_{ijkl} as follows

$$[\varphi] = \langle\sigma_{ij}\rangle\left[\varepsilon_{ij} - \varepsilon^p_{ij}\right]. \tag{12}$$

Thus, the expression for $\dot{\Phi}$ is obtained using Eqs. (9)–(11)

$$\dot{\Phi} = \int_V \sigma_{ij} \left(\dot{\varepsilon}_{ij} - \dot{\varepsilon}^p_{ij} \right) dV - \int_S [\varphi] \omega_N \, dS. \tag{13}$$

The expression of external power P_{ext} can be obtained after simplifications from Eq. (8)

$$P_{ext} = \int_V \sigma_{ij} \dot{\varepsilon}_{ij} \, dV - \int_S \langle \sigma_{ij} \rangle [\varepsilon_{ij}] \, \omega_N \, dS + \int_S \langle \sigma_{ij} n_j \rangle [v_i]^{(2)} \, dS. \tag{14}$$

By comparing Eqs. (13) and (14), the total dissipation D of the system is positive and reads according to Eq. (6)

$$D = \int_V \sigma_{ij} \dot{\varepsilon}^p_{ij} \, dV - \int_S \left(\langle \sigma_{ij} \rangle [\varepsilon_{ij}] - [\varphi] \right) \omega_N \, dS + \int_S \langle \sigma_{ij} n_j \rangle [v_i]^{(2)} \, dS. \tag{15}$$

For homogeneous elastic properties, Eq. (12) can be applied so that Eq. (15) simplifies into

$$D = \int_V \sigma_{ij} \dot{\varepsilon}^p_{ij} \, dV - \int_S \langle \sigma_{ij} \rangle \left[\varepsilon^p_{ij} \right] \omega_N \, dS + \int_S \langle \sigma_{ij} n_j \rangle [v_i]^{(2)} \, dS. \tag{16}$$

The first term in Eq. (15) is the classic bulk dissipation due to crystallographic slip evolution in crystals without surface of discontinuity. The second term in Eq. (15) is due to the propagation of surface discontinuities and can be related to shear-coupled GB migration. The associated driving force on the discontinuity surface S is given by $[\varphi] - \langle \sigma_{ij} \rangle [\varepsilon_{ij}]$ for heterogeneous elastic solids and simplifies into $-\langle \sigma_{ij} \rangle \left[\varepsilon^p_{ij} \right]$ for homogeneous elastic ones. This driving force can be related to the energy-momentum tensor $P_{lj} = \varphi \delta_{lj} - \sigma_{ij} u_{i,l}$ introduced by [22] through the jump relationship $[P_{lj}] n_j = \left([\varphi] - \langle \sigma_{ij} \rangle [\varepsilon_{ij}] \right) n_l$ for heterogeneous elastic solids. The last term in Eq. (15) or Eq. (16) is due to a possible incoherent interface authorizing tangential GB sliding (see Eq. (4).).

In the following, we first highlight the application of the continuum kinematics and thermodynamics frameworks to stress-induced shear-coupled GB migration. From the continuum mechanics viewpoint, GB is here considered as a continuously distributed dislocation (in the sense of collective continuum defects) for both LAGB and HAGB. In Sect. 16.3, the transport of GB dislocations is fully examined considering a bicrystal with planar GB and average mechanical fields in each crystal.

3 Shear-Coupled GB Migration with Infinite Plane Grain Boundaries

3.1 Dissipation and Transport Equations

In this part and in the rest of the paper, interfacial sliding will be disregarded, and we only focus on stress-induced motion of discontinuity surfaces like GB, assuming they are coherent interfaces. This means that only the first two terms of Eq. (15) are considered. This situation corresponds to "perfect shear-coupling" GB migration as defined in [4]. Thus, for planar bi-crystalline systems, such as the one represented in Fig. 2, Eq. (15) yields

$$\frac{D}{V} = f\sigma_{ij}^{I}\dot{\varepsilon}_{ij}^{pI} + (1-f)\sigma_{ij}^{II}\dot{\varepsilon}_{ij}^{pII} + \left([\varphi] - \langle\sigma_{ij}\rangle[\varepsilon_{ij}]\right)\dot{f}, \tag{17}$$

where f is the current volume fraction of crystal I. If crystal I moves into crystal II, $\dot{f}$ describes the rate of growth of the thickness of crystal I due to normal motion. In the particular case of homogeneous elasticity, $[\varphi] - \langle\sigma_{ij}\rangle[\varepsilon_{ij}]$ should be replaced by $-\langle\sigma_{ij}\rangle\left[\varepsilon_{ij}^{p}\right]$ in Eq. (17). Furthermore, the overall strain (resp. stress) evolution are given by the following transport equations (see also [23]) involving the strain (resp. stress) jump $\left[\varepsilon_{ij}\right]$ (resp. $\left[\sigma_{ij}\right]$) for the plane discontinuity surface S

$$\dot{E}_{ij} = \frac{1}{V}\int_{V}\dot{\varepsilon}_{ij}\,dV - \frac{1}{V}\int_{S}\left[\varepsilon_{ij}\right]\omega_N\,dS = f\dot{\varepsilon}_{ij}^{I} + (1-f)\dot{\varepsilon}_{ij}^{II} - \left[\varepsilon_{ij}\right]\dot{f}, \tag{18}$$

$$\dot{\Sigma}_{ij} = \frac{1}{V}\int_{V}\dot{\sigma}_{ij}\,dV - \frac{1}{V}\int_{S}\left[\sigma_{ij}\right]\omega_N\,dS = f\dot{\sigma}_{ij}^{I} + (1-f)\dot{\sigma}_{ij}^{II} - \left[\sigma_{ij}\right]\dot{f}. \tag{19}$$

From Eq. (18) and assuming homogeneous elasticity, the overall plastic strain rate reads

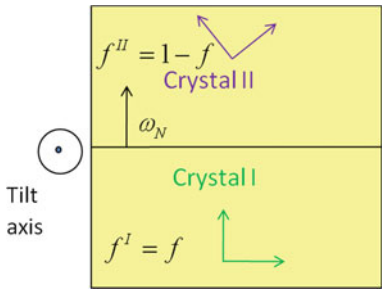

Fig. 2 Bicrystal configuration for shear-coupled GB migration with infinite planar interface (GB plane). Here, the consumed grain (crystal II) is chosen as the reference lattice

$$\dot{E}^{p}_{ij} = \frac{1}{V}\int_{V} \dot{\varepsilon}^{p}_{ij}\,dV - \frac{1}{V}\int_{S} \left[\varepsilon^{p}_{ij}\right]\omega_N\,dS = f\dot{\varepsilon}^{pI}_{ij} + (1-f)\dot{\varepsilon}^{pII}_{ij} - \left[\varepsilon^{p}_{ij}\right]\dot{f} \quad (20)$$

For an infinite plane discontinuity surface and considering heterogeneous elasticity, the strain concentration equations (given an applied overall strain for instance) are detailed in [24]. The calculations give the following general expressions for ε^{I}_{ij} and ε^{II}_{ij}

$$\begin{aligned} \varepsilon^{I}_{ij} &= A^{I}_{ijkl}E_{kl} - (1-f)\,G_{ijkl}\left[\sigma^{p}_{kl}\right], \\ \varepsilon^{II}_{ij} &= A^{II}_{ijkl}E_{kl} + fG_{ijkl}\left[\sigma^{p}_{kl}\right], \end{aligned} \quad (21)$$

where E_{ij} are the overall homogeneous strains, A^{I}_{ijkl}, A^{II}_{ijkl} are respectively the strain concentration tensors for crystals I and II, G_{ijkl} is a strain influence tensor which depends on the anisotropic elastic constants in crystals I and II. In Eq. (21), $\left[\sigma^{p}_{ij}\right]$ is defined by

$$\left[\sigma^{p}_{ij}\right] = C^{II}_{ijkl}\varepsilon^{pII}_{kl} - C^{I}_{ijkl}\varepsilon^{pI}_{kl}. \quad (22)$$

A^{I}_{ijkl}, A^{II}_{ijkl}, $\left[\sigma^{p}_{ij}\right]$ and G_{ijkl} are given in [24]. The strain jump $[\varepsilon_{ij}]$ can be easily derived from Eq. (21). In addition, the effective (overall) elastic moduli C^{eff}_{ijkl} of the bicrystal can be computed using Eq. (21) together with $\left[\sigma^{p}_{ij}\right] = 0$ and the static averaging rules. The complete expressions of the effective elastic moduli C^{eff}_{ijkl} are given elsewhere [24].

In Eq. (17), the term $\left([\varphi] - \langle\sigma_{ij}\rangle[\varepsilon_{ij}]\right)\dot{f}$ (general case) or $-\langle\sigma_{ij}\rangle\left[\varepsilon^{p}_{ij}\right]\dot{f}$ (for homogeneous elasticity) has to be expressed. These terms characterize the intrinsic dissipation per unit volume due the shear-coupled GB migration mechanism. In the following, the link between continuum-based GB dislocation density and the coupling factor β is recalled using the continuum dislocation density tensor introduced by [25] and [26].

3.2 GB Dislocation Densities and β Coupling Factor

In the continuum dislocation theory [25–27], the dislocation density tensor α_{hi} is defined as the *Curl* of the incompatible elastic distortion β^{e}_{ji} (i.e. the elastic incompatible part of the displacement gradient $u_{i,j} = \beta_{ji} = \beta^{e}_{ji} + \beta^{p}_{ji}$ in the linearized theory) as follows

$$\alpha_{hi} = \in_{hlj}\beta^{e}_{ji,l}, \quad (23)$$

where $\in_{hlj}$ is the permutation tensor. According to the Frank-Bilby theory of surface dislocations [6–8], the plastic distortion jump (or *eigendistortion*) due to the GB

dislocations (which is a continuum description of discrete GB defects present at the atomic scale and responsible for GB migration) can be obtained from the expression of surface dislocation densities [8, 28] defined as follows

$$\alpha^{S}_{hi} = \in_{hlj}\left[\beta^{e}_{ji}\right] n_l = \in_{hlj}\left(\beta^{eII}_{ji} - \beta^{eI}_{ji}\right) n_l. \tag{24}$$

Applying the 1st order Hadamard compatibility relation [19] at the discontinuity surface (i.e. $\in_{hlj}\left[\beta_{ji}\right] n_l = \in_{hlj}\left(\beta^{II}_{ji} - \beta^{I}_{ji}\right) n_l = 0$) , Eq. (24) yields

$$\alpha^{S}_{ij} = -\in_{jkl}\left[\beta^{p}_{li}\right] n_k. \tag{25}$$

Assuming t_l a given unit vector in the boundary plane (of unit normal n_m) in Fig. 3 and w_j a unit vector such as $w_j = \in_{jmn} n_m t_n$, then the resultant Burgers vector of dislocation lines cut by t_l is $B_i = \alpha^{S}_{ij} w_j$. Using Eq. (25), $\in_{jkl}\in_{jmn} = \delta_{km}\delta_{ln} - \delta_{kn}\delta_{lm}$ and $n_n t_n = 0$, it comes

$$B_i = -\left[\beta^{p}_{li}\right] t_l. \tag{26}$$

The plastic distortion jump $\left[\beta^{p}_{li}\right]$ results from plastic accommodation due the motion of gliding surface dislocation embodied by α^{S}_{ij}. This formalism was first applied to martensitic transformations by [8] and later by [2] for "shear-coupled" GB migration. If crystal II is consumed during the motion of crystal I into crystal II then crystal II will be considered as the reference lattice. This is similar to a parent phase in martensitic transformations as described in [8]. Thus,

$$\left[\beta^{p}_{li}\right] = -\beta l_i g_l, \tag{27}$$

where l_i and g_l are unit vectors defined with respect to the reference crystal (see Fig. 3) so that the interface dislocations can be considered for LAGB as discrete distributions of straight dislocations parallel to a unit vector. For HAGB, the interface dislocations are general surface dislocations. Eq. (27) characterizes a simple shear of magnitude β defined as the "coupling factor" by [4] during perfect shear-coupled GB migration (i.e. without sliding). This β factor was already identified in Sect. 2.1

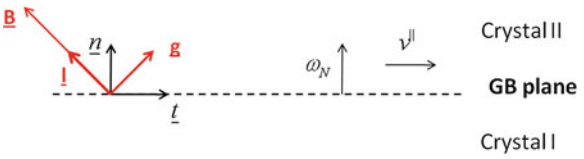

Fig. 3 Definition of surface dislocation Burgers vector B_i with respect to reference crystal II. l_i is a unit vector in the direction of the Burgers vector, and g_i represents the unit normal to the gliding plane of the surface dislocation

without making any reference to the surface dislocation concept like in the present section.

Here, l_i gives the direction of the Burgers vector content B_i such that $B_i = Bl_i$, where B is its magnitude, and g_i represents the unit normal to the gliding plane of the GB dislocations, such as Eqs. (26) and (27) give

$$B_i = \beta l_i g_l t_l = B l_i. \tag{28}$$

From the last equation, the relationship between B and β is found

$$\beta = \frac{B}{g_l t_l} \tag{29}$$

In the case of STGB with a tilt axis direction given by the unit vector

$$p_j = \epsilon_{jmn} l_m g_n = \epsilon_{jmn} t_m n_n,$$

simple geometric considerations using Fig. 3 gives the expression of the coupling factor

$$\beta = \frac{B}{l_l n_l}. \tag{30}$$

This relationship is consistent with [1]'s work through their *Eq. (21)*. In this section, the most important is the expression of $\left[\varepsilon^p_{ij}\right]$, the symmetric part of $\left[\beta^p_{ji}\right]$, which reads from Eq. (27)

$$\left[\varepsilon^p_{ij}\right] = -\widetilde{R_{ij}}\beta \tag{31}$$

with

$$\widetilde{R_{ij}} = \frac{1}{2}\left(l_i g_j + g_i l_j\right). \tag{32}$$

$\widetilde{R_{ij}}$ is defined as the "orientation tensor" associated to the shear deformation (or slip) of magnitude β coupled to GB migration. From the previous definitions of l_i and g_j in Fig. 3, $\widetilde{R_{ij}}$ and $\left[\varepsilon^p_{ij}\right]$ are traceless (i.e. $\widetilde{R_{kk}} = 0$) so that the induced plastic strain due to shear-coupled GB migration is incompressible.

3.3 Thermodynamic Driving Forces

From Eq. (17), the total dissipation per unit volume can be rewritten in the following general form

$$\frac{D}{V} = F_i\left(E_{kl}, \Sigma_{kl}, X_j\right)\dot{X}_i, \tag{33}$$

where F_i are the driving forces associated to internal variables X_i. These ones depend on the overall strains E_{ij} or stresses Σ_{ij} and on the three internal variables X_j (i.e. $\varepsilon_{ij}^{pI}, \varepsilon_{ij}^{pII}, f$). In this problem, the three driving forces $F_{\varepsilon^{pI}}, F_{\varepsilon^{pII}}, F_f$ associated respectively to $\varepsilon_{ij}^{pI}, \varepsilon_{ij}^{pII}, f$ (describing three independent inelastic processes) are listed below using Eq. (17)

$$\begin{aligned} F_{\varepsilon^{pI}} &= f\sigma_{ij}^{I}, \\ F_{\varepsilon^{pII}} &= (1-f)\,\sigma_{ij}^{II}, \\ F_f &= [\varphi] - \langle\sigma_{ij}\rangle\,[\varepsilon_{ij}], \end{aligned} \tag{34}$$

where $\sigma_{ij}^{I}, \sigma_{ij}^{II}, \langle\sigma_{ij}\rangle, [\varphi]$ and $[\varepsilon_{ij}]$ can be computed using Eq. (21). In the case of homogeneous elasticity without intra-crystalline slip, F_f simply becomes $F_f = -\langle\sigma_{ij}\rangle\left[\varepsilon_{ij}^{p}\right] = \langle\sigma_{ij}\rangle\widetilde{R_{ij}}\beta = \tilde{\tau}\beta$ following Sect. 3.2, where $\tilde{\tau}$ is the driving resolved shear stress on the surface dislocation gliding plane associated to $\left[\varepsilon_{ij}^{p}\right]$, $\widetilde{R_{ij}}$ is the orientation tensor previously defined in Sect. 3.2 and β is the shear coupling factor.

In the thermo-mechanics of plasticity [29, 21], the critical forces (corresponding to "threshold stresses" for the previous irreversible processes) are needed to complete the theory. The considered constitutive expressions for the critical forces and the kinetics law must be chosen with respect to a positive dissipation per unit volume in Eq. (33).

3.4 Critical Forces and Bi-Crystal's Overall Behavior

If the critical forces for intra-crystalline plastic deformation in both crystals ε_{ij}^{pI}, ε_{ij}^{pII}, f, here denoted $F_{\varepsilon^{pI}}^{C}, F_{\varepsilon^{pII}}^{C}$, are higher than their respective corresponding driving forces and only the critical force for shear-coupled GB migration denoted F_f^C is reached by F_f then

$$\begin{aligned} F_{\varepsilon^{pI}} &< F_{\varepsilon^{pI}}^{C}, \\ F_{\varepsilon^{pII}} &< F_{\varepsilon^{pII}}^{C}, \\ F_f &= F_f^C \end{aligned} \tag{35}$$

In the case of homogeneous elasticity, the last equation in Eq. (35) reduces to $\tilde{\tau} = \widetilde{\tau_C}$ for a given shear coupling factor β, where $\widetilde{\tau_C}$ is the critical shear stress resolved on the surface dislocation gliding plane. When F_f reaches F_f^C (or when $\tilde{\tau}$ reaches $\widetilde{\tau_C}$ in the case of homogeneous elasticity) in Eq. (35), the GB migration flux is given by the expression of $\dot{f}$ for an infinite GB plane as follows

$$\dot{f} = \frac{1}{V}\int_S \omega_N\,dS = \frac{\omega_N S}{V} = \frac{\omega_N}{L}, \tag{36}$$

where L is the total length of the deformed bicrystal in the normal direction to the GB.

The overall Hooke's law together with Eqs. (18), (19), (36) give the following constitutive relationship between the overall stress and strain rates

$$\dot{\Sigma}_{ij} = C^{eff}_{ijkl}\left(\dot{E}_{kl} + \frac{\omega_N}{L}\left([\varepsilon_{kl}] - S^{eff}_{klmn}[\sigma_{mn}]\right)\right), \tag{37}$$

where $[\sigma_{ij}]$ and $[\varepsilon_{ij}]$ are provided by Eq. (21) depending on homogeneous stress or strain conditions prescribed at the boundary of the bicrystal. Thus, for heterogeneous elastic bicrystals, Eq. (37) also writes

$$\dot{\Sigma}_{ij} = C^{eff}_{ijkl}\left(\dot{E}_{kl} - \dot{E}^{peff}_{kl}\right), \tag{38}$$

where $\dot{E}^{peff}_{ij}$ is the effective (overall) plastic strain rate due to shear-coupled GB migration defined as

$$\dot{E}^{peff}_{ij} = -\frac{\omega_N}{L}\left([\varepsilon_{ij}] - S^{eff}_{ijkl}[\sigma_{kl}]\right). \tag{39}$$

If homogeneous elasticity is assumed, the constitutive law simplifies into

$$\dot{\Sigma}_{ij} = C_{ijkl}\left(\dot{E}_{kl} + \left[\varepsilon^{p}_{kl}\right]\frac{\omega_N}{L}\right), \tag{40}$$

which gives, using Eq. (31) in the case, where crystal II is consumed,

$$\dot{\Sigma}_{ij} = C_{ijkl}\left(\dot{E}_{kl} - \widetilde{R_{kl}}\beta\frac{\omega_N}{L}\right). \tag{41}$$

Following recent experimental data [30], stress-driven shear-coupled GB migration exhibits a temperature dependence indicating that a thermally-activated process is at the origin of the shear-coupled GB migration. It is noteworthy that recent efforts were made to capture the kinetics law for the GB migration process at finite temperatures and strain rates by [11]. However, the accurate determination of the kinetics parameters for the three investigated Cu STGB will need specific simulation methods (parallel-replica dynamics, nudged elastic band methods) which are out of the scope of the present study.

Equation (38) shows that once GB migration is active for a given normal velocity ω_N (which also depends on the applied velocity to the bicrystal), the instantaneous stress decrease due to induced plastic strain is dependent on the effective elastic moduli C^{eff}_{ijkl} (or C_{ijkl} in the case of homogeneous elasticity), the GB character (through $\widetilde{R_{ij}}$ and β) and the bicrystal finite size L. The calculation of $\dot{f}$ (or equivalently the volume fraction increment dictated by the stepwise normal GB motion at each GB migration event) will be specified and discussed in Sect. 4 (for 0 and 500 K temperatures) with application to particular [001] Cu STGB (coincident GB). For

the latter, the atomistic mechanisms and collective steps when GB migrates are known following appropriate vectors of the "displacement shift complete" (DSC) lattice [1, 14].

4 Application to Cu [001] Symmetric Tilt Grain Boundaries (STGB)

4.1 Shear Modes

Following [1, 2, 11], we considered [001] STGB in cubic metals like Cu (f.c.c. metal). GB are generally characterized by five angles. Four angles are set up by choosing the tilt axis and the GB plane is a particular mirror plane of the bi-crystal containing the tilt axis. The misorientation angle θ is defined as the tilt angle between the [100] directions of both crystals in the counterclockwise direction, with $0 < \theta < \pi/2$ due to the four-fold symmetry around the tilt axis. Hence, the GB plane lies along the bisector between the [100] directions like in Fig. 4.

Following [2], two mappings for the Burgers circuit allows two possible B_i and two associated "coupling modes" to be defined. The first "coupling mode" called the <100> mode (or "mode I") is such that l_i is parallel to the cube direction [010] of the reference lattice (crystal II) and the Frank-Bilby dislocation slip planes are (100) [2]. The slip plane is represented to the left of the GB normal in Fig. 4. For small θ (LAGB), the expressions for B_i and the associated dislocation density can be resolved by a discrete distribution of single lattice dislocations of Burgers vectors $b_i = a_L$ [010], where a_L is the lattice parameter. For LAGB, the critical stress is proportional to the glide component of the Peach-Koehler force required to initiate the collective glide of the arrays of GB dislocations [10]. There are two kinds of LAGB: either for small θ or for θ close to π/2 (i.e. $\varphi = \pi/2 - \theta$ near 0). The latter corresponds to the GB "mode II" migration (<110> mode), where l_i is parallel to the direction $[1\ \bar{1}0]$

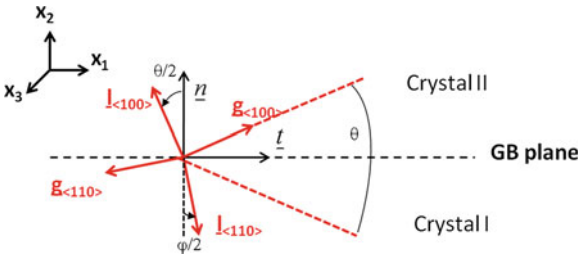

Fig. 4 Definition of the misorientation angle θ for [001]-type tilt boundaries. Two Burgers vectors B_i with directions given by unit vectors l_i are possible which correspond to two different mappings for Burgers circuit. The normal directions to the slip planes are given by unit vectors g_i. Angles θ and φ are linked each other by $\varphi = \pi/2 - \theta$

of the reference lattice (crystal I) and the associated resolved single dislocations are of type $B_i = a_L/2\left[1\bar{1}0\right]$. In this case, the Frank-Bilby surface dislocation glides along (110) planes, which is represented to the right of the GB normal in Fig. 4.

For HAGB, the discrete distributions of single dislocations can not be resolved anymore [31] and only the "Frank-Bilby equation" (Eq. (25)) is here used for these STGB. As established by [2], the Frank-Bilby equation (FBE) introduced in Sect. 3.2 provides two feasible solutions for [001] STGB and their continuous GB dislocation density.

These two solutions (as functions of θ) correspond to Burgers vectors either parallel to the [010] (denoted as B_i <100> for "mode I") or parallel to the $[1\bar{1}0]$ (denoted as B_i <110> for "mode II"). Here, [010] and $[1\bar{1}0]$ are crystallographic directions respectively defined in the crystal II and crystal I. For GB "mode I" migration, the consumed grain is crystal II (reference lattice) such as $\dot{f} \geqslant 0$, whereas for "mode II" migration, crystal I (reference lattice) is consumed with $\dot{f} \leqslant 0$. Under simple shear loading, these two coupling modes compete with each other, and the transition from one mode to the other occurs at a critical misorientation angle θ which depends on temperature (see Fig. 8 in [1]). Note that as the temperature drops, the θ range of "mode II" expands and it may be the only active coupling mode for all values of θ at $T = 0$ K. The invoked reason is that the activation of "mode I" requires the breaking of the mirror symmetry due to equivalent row translations by lattice vectors 1/2[001] and $1/2[00\bar{1}]$. This symmetry can only be broken at finite temperatures, where ledges and other defects may form easily. This issue was also checked using the gamma-surfaces associated to both modes at 0 K by [1].

Thus, due to the complexity of atomistic mechanisms in the case of general GB, we here limit atomistic investigations to study the constitutive behavior associated with the STGB shear-coupled migration. For this case, MD simulations are conducted for three Cu [001] STGB with misorientation angles $\theta = 77.32°, 53.13°, 28.07°$ which show the well-identified temperature dependent shear-coupling <100> and <110> modes linked to two characteristic coupling factors β (resp. positive and negative). According to [1], the coupling factor β depends on θ and on the "coupling modes" as follows

$$\begin{aligned} \beta_{<100>} &= 2\tan\left(\frac{\theta}{2}\right), \\ \beta_{<110>} &= -2\tan\left(\frac{\varphi}{2}\right), \end{aligned} \tag{42}$$

where $\varphi = \frac{\pi}{2} - \theta$. The atomistic MD simulations which are shown in Sect. 4.2 will first provide the shear stress response, the temperature dependent shear coupling mode as a function of the GB character, the critical shear stresses (or "peak stresses"), the stress accommodation due to shear (shear stress drop during GB migration) and the saw-tooth behavior (stick slip character). Second, the results of the developed micromechanics-based model regarding elastic slopes and shear stress drops will

be discussed in Sect. 4.3. The roles of GB character, bicrystal size and cubic elastic anisotropy will be studied in Sect. 4.3.

4.2 Molecular Dynamics (MD) Simulations

In this subsection, a few "flat" Cu [001] STGB, namely Σ41(540) ($\theta = 77.32°$), Σ5(210) ($\theta = 53.13°$), Σ17(410) ($\theta = 28.07°$), were studied at 0 K and at 500 K temperatures using the EAM interatomic potential provided by [32] for Cu. Note that in the work of [1], where MD simulations were performed under simple shear loading at 800 K, the first two STGB display "mode II" migration, and the last one displays the "mode I" (see Table 3.1 in [1]). However, all of them display the "mode II" (<110> mode) at 0 K as can be inferred from the plots in the Fig. 8 of [1]. Here, each bi-crystal with [001] STGB is created using the coincident site lattice (CSL) model by placing the first crystal on the top of the other using the following procedure (Fig. 5). The tilt axis (x3-axis) is along [001] direction. The horizontal plane (x1,x3) corresponds to the GB plane, and [100] directions for crystals I and II makes an angle θ. The gap between the two crystals is set to about 2 Angström before it is subjected to energy minimization. Several initial configurations are also tested by shifting the upper grain with respect to the lower along the (x1) direction so as to obtain the lowest energy state of a GB configuration after atomic relaxation. The energy minimization

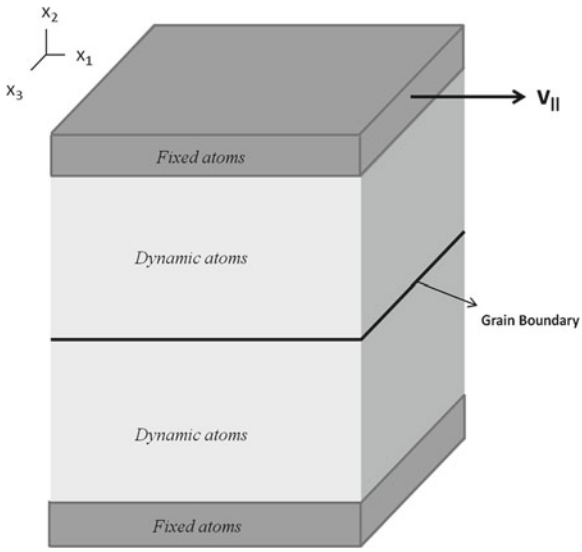

Fig. 5 Schematic figure of the computational atomistic unit cell box with coordinate axes and periodic boundary conditions. L is the total length in the normal direction (as defined in the text) to the GB plane for dynamic atoms subjected to shear

Table 1 Elastic shear moduli obtained by the MD results and by the present micromechanical model accounting for anisotropic elasticity for Σ41(540), Σ5(210), Σ17(410) [001] STGB

Effective elastic shear moduli (GPa)	Σ41(540)	Σ5(210)	Σ17(410)
Atomistic simulations	25.4	35.6	57.4
Present model (anisotropic)	25.7	39.5	61.8
Voigt-Reuss-Hill average (isotropic)	47.8	47.8	47.8

The isotropic Voigt-Reuss-Hill average is also given for comparisons

is performed with the LAMMPS simulator[1] using a conjugate gradient method. Each Cu crystal for simulations is approximately cubic shaped, and the simulation block for the bicrystal contains between 30000–45000 atoms with periodicity in the (x1) and the (x3) directions. After optimization, the relaxed structure is subjected to constant shear strain rate loading as follows. The simulation block (Fig. 5) is sandwiched between the top and the bottom layer (along the (x_2) axis) of thickness about 2 times the potential cut-off distance. These two layers do not participate in computing data from the simulations and serve only to impose simple shear loading. The bottom block is held fixed and the constant shear velocity $v_0 = v^{\parallel} = \dot{E}L$ is applied on the top part of the block in the (x_1) direction, where $\dot{E}$ is the constant shear strain rate ($\dot{E} = 10^8 s^{-1}$) and L is the simulation block length containing unconstrained atoms. Here, two different values were chosen to keep initial crystal characteristic sizes lower or equal to 10 nm to mimic nanocrystals, namely $L = 12.2$ nm and $L = 20$ nm. The time step is 1 fs. These simulations are conducted at 0.001 K and at 500 K, and the overall stress tensor was computed using the standard virial expression averaged over all dynamic atoms. The GB position was also tracked from the common neighborhood analysis (CNA) computation. The CNA value for atoms in f.c.c. lattice is 1 and for atoms forming GB structural units it is 5 [33, 34].

4.3 Discussion of the Continuum Model and Comparisons with MD Results

The micromechanics-based approach is applied to the three previously investigated Cu bi-crystals with [001] STGB. The motivation to study Cu bi-crystals lies in the fact that they exhibit a strongly anisotropic elastic behavior characterized by the following anisotropic coefficient $a = \dfrac{2C_{44}}{C_{11} - C_{12}} = 3.26$. The cubic elastic moduli for Cu are taken as $C_{11} = 170$ GPa, $C_{12} = 122.5$ GPa and $C_{44} = 76$ GPa. These elastic constants are given by [32] and were used by these authors to validate the EAM potential for Cu. In this paper, the application of the micromechanics-based theory is mainly focused on the effect of elastic anisotropy on the shear stress-strain curves before and at the first shear-coupled GB migration event (Fig. 6).

[1] LAMMPS Molecular Dynamics Simulator; http///lammps.sandia.gov/.

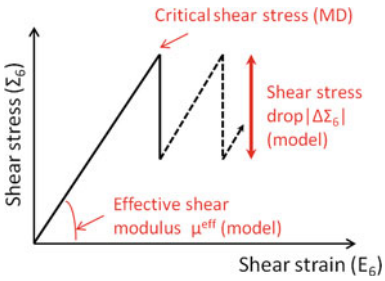

Fig. 6 Schematic representation of the shear stress versus shear strain curve and the quantitative values predicted by the micromechanical model: elastic slopes and shear stress drops. The critical shear stress (also called "peak stress") is obtained by MD simulations

For homogeneous isotropic elastic properties, the isotropic elastic coefficients for Cu are obtained using the classic "Voigt-Reuss-Hill average" model [35]. This model gives $\mu = 47.8$ GPa (isotropic elastic shear modulus) and $\nu = 0.345$ (Poisson ratio). The isotropic shear modulus is reported on Table 1 for comparisons with the effective elastic shear moduli μ^{eff} derived for general elastic anisotropy [24]. The numerical values for elastic moduli are computed in both crystals using the cubic symmetry for $\Sigma41(540)$ ($\theta = 77.32°$), $\Sigma5(210)$ ($\theta = 53.13°$), $\Sigma17(410)$ ($\theta = 28.07°$) that can be used to derive the effective elastic moduli for the three investigated bi-crystals. We find for $f = 1 - f$ (initial elastic slope) that the effective elastic shear moduli (Table 1) are in good agreement with the atomistic simulations at 0 K and at 500 K. In contrast, we remark that the classic isotropic assumption obtained from "Voigt-Reuss-Hill average" is sometimes far from the atomistic results for the studied Cu [001] STGB, which means that the simple elastic isotropic assumption is not realistic for the present application. The mechanical responses given by the micromechanical model can be enriched by the critical forces F_f^C or the critical resolved shear stresses on the GB slip plane $\widetilde{\tau_C}$ in Eq. (35) directly obtained from the peak stresses (or critical shear stresses τ_C) of the atomistic results (see Sect. 4.2). These peak stresses resulted from simple shear performed at an applied material velocity $v^{\parallel}$ parallel to the GB plane (Fig. 5).

Second, we focus on the analysis of shear stress drops in the light of the micromechanical approach after the first GB migration event, i.e. for $f = 1 - f$ in the constitutive model assuming isotropic elasticity or fully anisotropic elasticity in both crystals. Following MD results detailed in [24], we start by the analysis of first shear stress drops when the "mode II" (<110> mode) is activated at 0 K for the three GBs and at 500 K for $\Sigma41(540)$ and $\Sigma5(210)$. Then, the model is applied to the case when the "mode I" (<100> mode) is activated at 500 K for $\Sigma17(410)$. Lastly, the model is applied to understand the origin of bi-crystal size effects on stress drops at 0 K for the three STGBs.

As seen from atomistic simulations, "mode II" is a dominating shear mode especially at 0 K for the three GBs. According to Fig. 4, l_i and g_i are defined so that the <110> mode ("mode II") is characterized by

$$l_i n_i = g_i t_i = -\cos\left(\frac{\varphi}{2}\right) = -\cos\left(\frac{\pi}{4} - \frac{\theta}{2}\right)$$

which gives

$$l_i = \left(\sin\left(\frac{\pi}{4} - \frac{\theta}{2}\right), -\cos\left(\frac{\pi}{4} - \frac{\theta}{2}\right), 0\right)$$

and

$$g_i = \left(-\cos\left(\frac{\pi}{4} - \frac{\theta}{2}\right), -\sin\left(\frac{\pi}{4} - \frac{\theta}{2}\right), 0\right)$$

and $\widetilde{R_{ij}}$ from Eq. (32). Since crystal I is the parent grain, only crystal II undergoes plastic deformation, thus $\left[\varepsilon_{ij}^{p}\right] = \varepsilon_{ij}^{pII} = -\widetilde{R_{ij}}\beta$. When the critical shear stress is reached, shear-coupled GB migration is active. Then, time integration of Eq. (38) during the first shear-coupled GB migration event yields

$$\dot{\Sigma}_{ij}\delta t = C_{ijkl}^{eff}\dot{E}_{kl}\delta t + \frac{h_N}{L}\left(C_{ijkl}^{eff}\left[\varepsilon_{kl}\right] - \left[\sigma_{ij}\right]\right). \tag{43}$$

From atomistic results, the step time δt for each single shear-coupled GB migration event is a few *ps*. This time scale is out of the scope of continuum mechanics for which GB migration is seen as instantaneous. In Eq. (43), the strain and stress jumps (resp. $[\varepsilon_{ij}]$ and $[\sigma_{ij}]$) can be computed using Eq. (21) for homogeneous stress or strain boundary conditions. These jumps depend on the elastic properties of both crystals and depend on $\widetilde{R_{ij}}$ and β. In Eq. (43), h_N denotes the normal step height during stepwise GB motion (at the first GB migration event) which corresponds to the characteristic step height due to GB disconnection loop nucleation [15]. In the case of "mode II", the GB plane moves down (negative motion with respect to the (x_2) axis in Fig. 5) to a new position when τ_C is reached for which the activation energy for GB migration is overcome. At this point, the second term in Eq. (43), that contains the strain and stress jumps, h_N and the effective elastic moduli, is responsible for shear stress drop when migration is active. Without trying to determine the complete activation energy profile for the three studied STGB, the transition from an unstable state to a metastable state associated with the dissipative GB migration event is then described by a normal step height h_N. This characteristic distance h_N is also linked to the DSC lattice vector following for coincident (CSL) GB. The DSC ("displacement shift complete") lattice is the largest lattice including all the sites of the lattices of both crystals. According to [14, 1], the disconnection step height h_N is linked to the DSC lattice spacing. Thus, the expression of the disconnection step height h_N depends on the GB character (through θ) and on the lattice parameter a_L. For the $<110>$ mode, h_N is negative and is given by [1]

$$h_N{}^{<110>} = -\frac{a_L}{\sqrt{2}}\cos\left(\frac{\varphi}{2}\right), \tag{44}$$

Table 2 Normal step height h_N average values obtained by Eq. (44) (theory) compared to MD results for Cu Σ41(540), Σ5(210), Σ17(410) [001] STGB

h_N (nm) for <110> mode	Σ41(540)	Σ5(210)	Σ17(410)
Atomistic simulations (average values)	–0.255	–0.248	–0.220
Theory (for present model)	–0.254	–0.242	–0.219

where $a_L = 0.3615\,\text{nm}$ for Cu. The numerical values obtained for h_N from MD simulations are computed by averaging the different GB position steps. The comparisons between these values and the theoretical ones given by Eq. (44) are provided in Table 2 and show a very good agreement.

Here, the shear-coupled GB migration event is assumed instantaneous at the continuum mechanics time scale so that during the stepwise GB motion $\Delta E_{ij} = \dot{E}_{ij}\delta t = 0$ in Eq. (43), thus

$$\Delta\Sigma_{ij} = \frac{h_N}{L}\left(C^{\text{eff}}_{ijkl}\,[\varepsilon_{kl}] - [\sigma_{ij}]\right). \tag{45}$$

Assuming linear isotropic homogeneous elasticity, Eq. (45) simplifies into

$$\Delta\Sigma_{ij} = -2\mu\frac{h_N}{L}\beta\widetilde{R_{ij}} \tag{46}$$

since $\widetilde{R_{kk}} = 0$ (see Sect. 3.2).

In the following, the tensor to matrix convention is used. The pairs of subscripts ij and kl are converted to single subscripts as follows: $11\rightarrow 1$, $22\rightarrow 2$, $33\rightarrow 3$, 23 and $32\rightarrow 4$, 13 and $31\rightarrow 5$, 12 and $21\rightarrow 6$. For simple shear parallel to GB plane in the (x_1) direction as performed in the MD simulations (Fig. 5), the shear stress increment is obtained from Eq. (45) as follows

$$\Delta\Sigma_6 = \frac{h_N}{L}\left(C^{\text{eff}}_{62}\,[\varepsilon_2] + C^{\text{eff}}_{64}\,[\varepsilon_4] + C^{\text{eff}}_{66}\,[\varepsilon_6]\right) \tag{47}$$

since $[\sigma_6] = 0$. Thus, the strain concentration equations (Eq. (22)) are here applied. For isotropic elasticity, Eq. (46) simply yields

$$\Delta\Sigma_6 = -\mu\frac{h_N}{L}\beta\widetilde{R_6} \tag{48}$$

with $\widetilde{R_6} = l_1 g_2 + g_1 l_2 = \cos\left(\frac{\pi}{2} - \theta\right)$.

The present micromechanics-based model is able to describe the shear stress drop magnitude in the stick-slip behavior (Fig. 6). The shear stress drop magnitude can be defined as the absolute value of the shear stress increment $|\Delta\Sigma_6|$ obtained from Eq. (47) or Eq. (48). The stick-slip behavior is dependent on the grain boundary char-

Table 3 Shear stress drop magnitudes (in MPa) obtained by the MD results at 0 and 500 K and by the micromechanical model with anisotropic and isotropic elastic formulations for Cu Σ41(540), Σ5(210), Σ17(410) [001] STGB with $L = 12.2$ nm

$\lvert\Delta\Sigma_6\rvert$ (MPa) for $L = 12.2$ nm	Σ41(540) (0K,500K)	Σ5(210) (0K,500K)	Σ17(410) (0K)
Atomistic simulations	100	417	1080
Present model (anisotropic)	127	603	1024
Present model (isotropic)	216	506	485

acter (through θ), the effective elastic properties of the bicrystal, the lattice parameter (through h_N) and the bicrystal finite size L. The numerical values regarding shear stress drop magnitudes for Σ41(540) ($\theta = 77.32°$), Σ5(210) ($\theta = 53.13°$), Σ17(410) ($\theta = 28.07°$) are reported in Table 3 both from atomistic results and from the micromechanical approach (either Eq. (47) for anisotropic elasticity or Eq. (48) for isotropic elasticity). The $\beta_{<110>}$ coupling factors are respectively −0.222, −0.667, −1.200 for Σ41(540), Σ5(210), Σ17(410). The quantitative comparisons reported in Table 3 give reasonable agreement with the atomistic results in the case of anisotropic elasticity for the three investigated STGB. In this case, the relative errors with respect to MD results appear to be quite acceptable. Conversely, the isotropic elasticity assumption give unrealistic results which are far from the MD results especially for Σ41(540) STGB, where the relative error reaches ~120 %. The results show that the isotropic elastic assumption may only be relevant for the particular case of Σ5(210) STGB, where both fully anisotropic and isotropic elastic formulations give similar values.

Another example, where the micromechanical approach can be applied, is the specific Cu Σ13 (320) ($\theta = 67.4°$) STGB investigated by [11]. In this case, the shear stress drop magnitude obtained by the authors using atomistic simulations at 0 K with $L = 6$ nm was found to be ~450 MPa [11]. Taking into account anisotropic elasticity (Eq. (47)) and the fact that the "mode II" is active at 0 K (Eq. (44)), the present model gives $|\Delta\Sigma_6| = 573$ MPa, which represents a relative error of ~27 %.

For Cu Σ17 (410) STGB, "mode I" occurs at 500 K according to MD results [24]. In this <100> mode, B_i (or l_i) forms an angle $\theta/2$ counterclockwise with respect to n_i (Fig. 4) such that

$$l_i n_i = g_i t_i = \cos\left(\frac{\theta}{2}\right), \qquad l_i = \left(-\sin\left(\frac{\theta}{2}\right), \cos\left(\frac{\theta}{2}\right), 0\right),$$

$$g_i = \left(\cos\left(\frac{\theta}{2}\right), \sin\left(\frac{\theta}{2}\right), 0\right).$$

Here, crystal II is the parent grain and only crystal I undergoes plastic deformation, thus $\left[\varepsilon_{ij}^{p}\right] = -\varepsilon_{ij}^{pI} = -\widetilde{R_{ij}}\beta$, where $\widetilde{R_{ij}}$ is given by Eq. (32). In this case, the first shear stress drop obtaind by MD simulations is ~300 MPa. The micromechanical model can also be applied in the same way to the "mode I" observed at $T = 500$ K.

Table 4 Shear stress drop magnitudes (in MPa) obtained by the MD results and by the micromechanical model with anisotropic and isotropic elastic formulations for Cu Σ41(540), Σ5(210), Σ17(410) [001] STGB with $L = 20\,nm$ at 0 K

$\lvert\Delta\Sigma_6\rvert$ (MPa) for $L = 20\,nm$	Σ41(540)	Σ5(210)	Σ17(410)
Atomistic simulations (0 K)	60	244	641
Present model (anisotropic)	78	368	624
Present model (isotropic)	132	309	296

In this case, the theoretical h_N value is now positive and is given by [1]

$$h_N{}^{<100>} = \frac{a_L}{2}\cos\left(\frac{\theta}{2}\right). \tag{49}$$

Using Eq. (47) (elastic anisotropy), we obtain $|\Delta\Sigma_6| = 322$ MPa, which represents a relative error of ~7 %.

It looks clear that the large discrepancies sometimes observed between the atomistic results and the model with the isotropic elastic assumption are mainly due to a poor estimate of the effective elastic shear modulus and the strains in both crystals.

Bicrystal size effect is observed in atomistic results on shear stress drop magnitude for Σ41(540), Σ5(210), Σ17(410). The results of the micromechanical model for $L = 20$ nm are given in Table 4 (for both isotropic and anisotropic formulations). Overall, the bicrystal size effect is well reproduced for both STGB in the case, where anisotropic elasticity is accounted for, especially for Σ41(540) and Σ17(410). Even though the micromechanical approach supposes mean strain and stress fields in both crystals (no intracrystalline shear stress fluctuations along the normal axis (x_2) to the GB plane), it is found that the bicrystal size effect (characterized by the internal length scale L) on the shear stress drop magnitude scales with $\frac{h_N}{L}$.

Here, h_N is fixed for a given STGB because it is linked to the lattice parameter a_L in Eq. (44). Following Eq. (47) and the fact that the terms $C_{62}^{eff}[\varepsilon_2] + C_{64}^{eff}[\varepsilon_4] + C_{66}^{eff}[\varepsilon_6]$ are not length scale dependent, the stress drop magnitude ratio $\frac{|\Delta\Sigma_6|_{L=12.2nm}}{|\Delta\Sigma_6|_{L=20nm}} = \frac{20}{12.2} \sim 1.64$ is in good agreement with the one obtained by atomistic simulations for Σ41(540), Σ5(210) and Σ17(410) which are respectively 1.67, 1.71 and 1.68 from Tables 3 and 4.

5 Conclusions

A new micromechanics-based model was investigated to describe shear-coupled GB migration in bicrystals. Both MD simulations (at 0 and 500 K) and a micromechanical model assuming Frank-Bilby GB dislocations were applied to three Cu [001]

STGB: $\Sigma 41(540)$ ($\theta = 77.32°$), $\Sigma 5(210)$ ($\theta = 53.13°$), $\Sigma 17(410)$ ($\theta = 28.07°$). The critical shear stresses for shear-coupled GB migration can be obtained by MD simulations. The role of Cu elastic anisotropy on the stick-slip features of shear-coupled migration has been observed on the shear stress-strain curves. These ones have been analyzed in the light of the micromechanical model. In this paper, both formulations including heterogeneous and homogeneous elasticity have been developed. It has been shown that the elastic shear moduli obtained by MD simulations are captured by the micromechanics-based model when heterogeneous elasticity is accounted for. Furthermore, the trends regarding shear stress drops during first shear-coupling GB migration event at 0 K and 500 K are well described by the micromechanical approach especially when anisotropic elasticity is considered in the formulation. The model may also be extended to various strain rates and temperatures assuming the shear-coupling modes can be easily identified by atomistic simulations. Interestingly, for very low velocities up to 5 m/s, the shear stress drop is not very sensitive to shear rates [11]. Advanced atomistic methods dedicated to the kinetics of shear-coupled migration should be developed to improve the constitutive kinetics law at finite temperatures for shear-coupled GB migration. It could also be interesting to compare/predict the experimental results although overall stress/strain curves are seldom reported. As some perspective, the present constitutive and computational framework developed for bi-crystals with shear-coupled GB migration will be applied to study stress-induced twin boundary migration and will be incorporated in polycrystalline continuum models.

Acknowledgments The authors are grateful to the French "Agence Nationale de la Recherche" under contract agreement ANR-07-BLAN-0186 for financial support.

References

1. Cahn, J.W., Mishin, Y., Suzuki, A.: Coupling grain boundary motion to shear deformation. Acta Mater. **54**, 4953–4975 (2006)
2. Cahn, J.W., Mishin, Y.: Duality of dislocation content of grain boundaries. Philos. Mag. **86**, 1–11 (2006)
3. Bobylev, S.V., Mozorov, N.F., Ovid'ko, I.A.: Cooperative grain boundary sliding and migration process in nanocrystalline solids. Phys. Rev. Lett. 105, 055, 504 (2010)
4. Cahn, J.W., Taylor, J.E.: A unified approach to motion of grain boundaries, relative tangential translation along grain boundaries and grain rotation. Acta Mater. **52**, 4887–4898 (2004)
5. Zhang, H., Du, D., Srolovitz, D.J.: Effects of boundary inclination and boundary type on shear-driven grain boundary migration. Philos. Mag. **88**, 243–256 (2008)
6. Frank, F.C.: In: Symposium on the plastic deformation of crystalline solids, pp. 150–154. Carnegie Institute of Technology, Pittsburgh (1950)
7. Bilby, B.A.: In: Bristol Conference Report on Defects in Crystalline Solids, pp. 124–133. The Physical Society of London (1955)
8. Bullough, R., Bilby, B.A.: Continuous distributions of dislocations: surface dislocations and the crystallography of martensitic transformations. Proc. Phys. Soc. B **69**, 1276–1286 (1956)

9. Tucker, G.J., Zimmerman, J.A., McDowell, D.L.: Continuum metrics for deformation and microrotation from atomistic simulations: application to grain boundaries. Int. J. Eng. Sci. **49**, 1424–1434 (2011)
10. Molodov, D.A., Gorkaya, T., Gottstein, G.: Low angle tilt boundary migration coupled to shear deformation. Acta Mater. **55**, 1843–1848 (2007)
11. Mishin, Y., Suzuki, A., Uberuaga, B.P., Voter, A.F.: Stick-slip mechanism of grain boundaries studied by accelerated molecular dynamics. Phys. Rev. B 75, 224, 101 (2007)
12. Ivanov, V.A., Mishin, Y.: Dynamics of grain boundary motion coupled to shear deformation: an analytical model and its verification by molecular dynamics. Phys. Rev. B 78, 064, 106 (2008)
13. Fischer, F.D., Schaden, T., Appel, F., Clemens, H.: Mechanical twins, their development and growth. Eur. J. Mech. A. Solids **22**, 709–726 (2003)
14. Rae, C.M.F., Smith, D.A.: On the mechanisms of grain boundary migration. Philos. Mag. A **41**, 477–492 (1980)
15. Hirth, J.P., Pond, R.C.: Steps, dislocations and disconnections as interface defects relating to structure and phase transformations. Acta Mater. **44**, 4749–4763 (1996)
16. Abeyaratne, R., Knowles, J.K.: On the driving traction acting on a surface of strain discontinuity in a continuum. J. Mech. Phys. Solids **38**, 345–360 (1990)
17. Cermelli, P., Gurtin, M.E.: The dynamics of solid-solid phase transitions-2. Incoherent interfaces. Arch. Rational. Mech. Anal. **127**, 41–99 (1994)
18. Fischer, F.D., Simha, N.K., Svoboda, J.: Kinetics of diffusional transformation in multicomponent elastic-plastic materials. J. Engng. Mater. Tech. **125**, 266–276 (1998)
19. Hadamard, J.: Lecons sur la propagation des ondes et les equations de l'hydrodynamique. College de France, Paris (1903)
20. Coleman, B.D., Gurtin, M.E.: Thermodynamics with internal state variables. J. Chem. Phys. **47**, 597–613 (1967)
21. Maugin, G.A.: Configurational forces: Thermomechanics. Mathematics and Numerics. CRC Press, Taylor and Francis, New York (2011)
22. Eshelby, J.D.: Energy relations and energy-momentum tensor in continuum mechanics. In: Kanninen, M., et al. (eds.) Inelastic Behaviour of Solids, pp. 77–115. McGraw-Hill, New York (1970)
23. Petryk, H.: Macroscopic rate-variables in solids undergoing phase transformation. J. Mech. Phys. Solids **46**, 873–894 (1998)
24. Berbenni, S., Paliwal, B., Cherkaoui, M.: A micromechanics-based model for shear-coupled grain boundary migration in bicrystals. Int. J. Plasticity (2013),http://dx.doi.org/10.1016/j.ijplas.2012.11.011
25. Nye, J.F.: Some geometrical relations in dislocated crystals. Acta Metall. **1**, 153–162 (1953)
26. Kröner, E.: Kontinuumstheorie der Versetzungen und Eigenspannungen. In: Collatz, L., Loesch, F. (eds.) Ergebnisse der Angewewandte Mathematik 5. Springer Verlag, Berlin (1958)
27. Willis, J.R.: Second-order effects of dislocations in anisotropic crystals. Int. J. Eng. Sci. **5**, 171–190 (1967)
28. Mura, T.: Micromechanics of defects in solids. Kluwer Academic Publishers, Dordrecht, The Netherlands (1987)
29. Rice, J.R.: Continuum mechanics and thermodynamics plasticity in relation to microscale deformation mechanisms. In: Argon, A.S. (ed.) Constitutive Equations in Plasticity, pp. 23–75. MIT Press, Cambridge (1975)
30. Gorkaya, T., Molodov, D.A., Gottstein, G.: Stress-driven migration of symmetrical [100] tilt grain boundaries in Al bicrystals. Acta Mater. **57**, 5396–5405 (2009)
31. Li, J.C.M.: High-angle tilt boundary-a dislocation core model. J. Appl. Phys. **32**, 525–541 (1961)
32. Mishin, Y., Mehl, M.J., Papaconstantopoulos, D.A., Voter, A.F., Kress, J.D.: Structural stability and lattice defects in copper: Ab initio, tight-binding, and embedded-atom calculations. Phys. Rev. B 63, 224, 106 (2001)

33. Faken, D., Jonsson, H.: Systematic analysis of local atomic structure combined with 3D computer graphics. Comput. Mater. Sci. **2**, 279–286 (1994)
34. Tsuzuki, H., Branicio, P.S., Rino, J.P.: Structural characterization of deformed crystals by analysis of common atomic neighborhood. Comp. Phys. Comm. **177**, 518–523 (2007)
35. Hill, R.: The elastic behaviour of a crystalline aggregate. Proc. Phys. Soc. Lond. **65**, 349–354 (1952)